

pubs.acs.org/journal/apchd5 Article

# Inverse-Designed Metastructures Together with Reconfigurable Couplers to Compute Forward Scattering

Vahid Nikkhah, Dimitrios C. Tzarouchis, Ahmad Hoorfar, and Nader Engheta\*



Cite This: ACS Photonics 2023, 10, 977-985



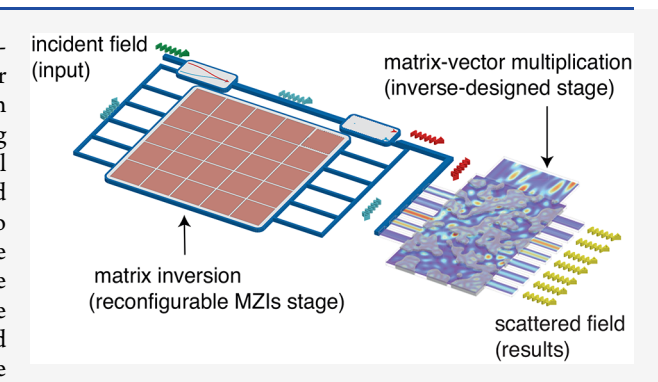
**ACCESS** I

III Metrics & More

Article Recommendations

Supporting Information

ABSTRACT: Wave-based analog computing in the forms of inverse-designed metastructures and the meshes of Mach—Zehnder interferometers (MZI) have recently received considerable attention due to their capability in emulating linear operators, performing vector-matrix multiplication, inverting matrices, and solving integral and differential equations via electromagnetic wave interaction and manipulation in such structures. Here, we combine these two platforms to propose a wave-based metadevice that can compute scattered fields in electromagnetic forward scattering problems. The proposed device consists of two subsystems: a set of reconfigurable couplers with a proper feedback system and an inverse-designed inhomogeneous material block. The first subsystem computes the magnitude and phase of the dipole polarization induced in the



scatterers when illuminated with a given incident wave (matrix inversion). The second subsystem computes the magnitude and phase of the scattered fields at given detection points (vector-matrix multiplication). We discuss the functionality of this metadevice, and through several examples, we theoretically evaluate its performance by comparing the simulation results of this device with full-wave numerical simulations and numerically evaluated matrix inversion. We also highlight that since the first section is reconfigurable, the proposed device can be used for different permittivity distributions of the scatterer and incident excitations without changing the inverse-designed section. Our proposed device may provide a versatile platform for rapid computation in various scattering scenarios.

KEYWORDS: metamaterial, inverse design, reconfigurability, emulator, scattering, MZI

# INTRODUCTION

Optical analog computing shows great promise for nextgeneration computing platforms. Owing to some of the features of light-matter interactions, optical metastructures give way for low-power and high-speed analog computations. <sup>1–5</sup> The artificially engineered electromagnetic structures known as metamaterials<sup>6</sup> combined with inverse-design techniques enable engineering of wave propagation through material structures down to subwavelength scales with unprecedented efficiency.<sup>7,8</sup> These structures can perform light-speed parallelized computations for complex computational problems such as solving integral equations. Moreover, the wave propagation through material structures exhibits parallelism in terms of encoding and processing information. 10,11 Considering the capabilities of optical analog computing, here we propose the idea of wave-based metadevices for performing specialized computational tasks, particularly for certain physical problems such as electromagnetic forward-scattering problems, which can be computationally very intensive.

In this work, we encode the information about the quantities of interest, that is, the complex-valued electric field and induced polarization in our scattering problem, into the complex amplitudes of the waveguide modes. Then, we process them by a metadevice, schematically shown in Figure 1, that consists of two subsystems. (a) A set of reconfigurable couplers, for example, Mach—Zehnder interferometers (MZIs), and (b) an inverse-designed metastructure. In the first part, a network of reconfigurable couplers is designed that, when endowed with a properly designed feedback loop, can compute the inverse of a given matrix. This part is designed to compute the magnitude and phase of the dipole polarization induced inside the target scatterers by the local electric field for a given incident field. As discussed below, since these couplers are tunable, the permittivity of implemented scatterers and the incident fields can be modified at will. The second part is an inverse-designed metastructure that performs a vector-matrix

Special Issue: Optimized Photonics and Inverse

Design

Received: March 7, 2022 Published: September 2, 2022





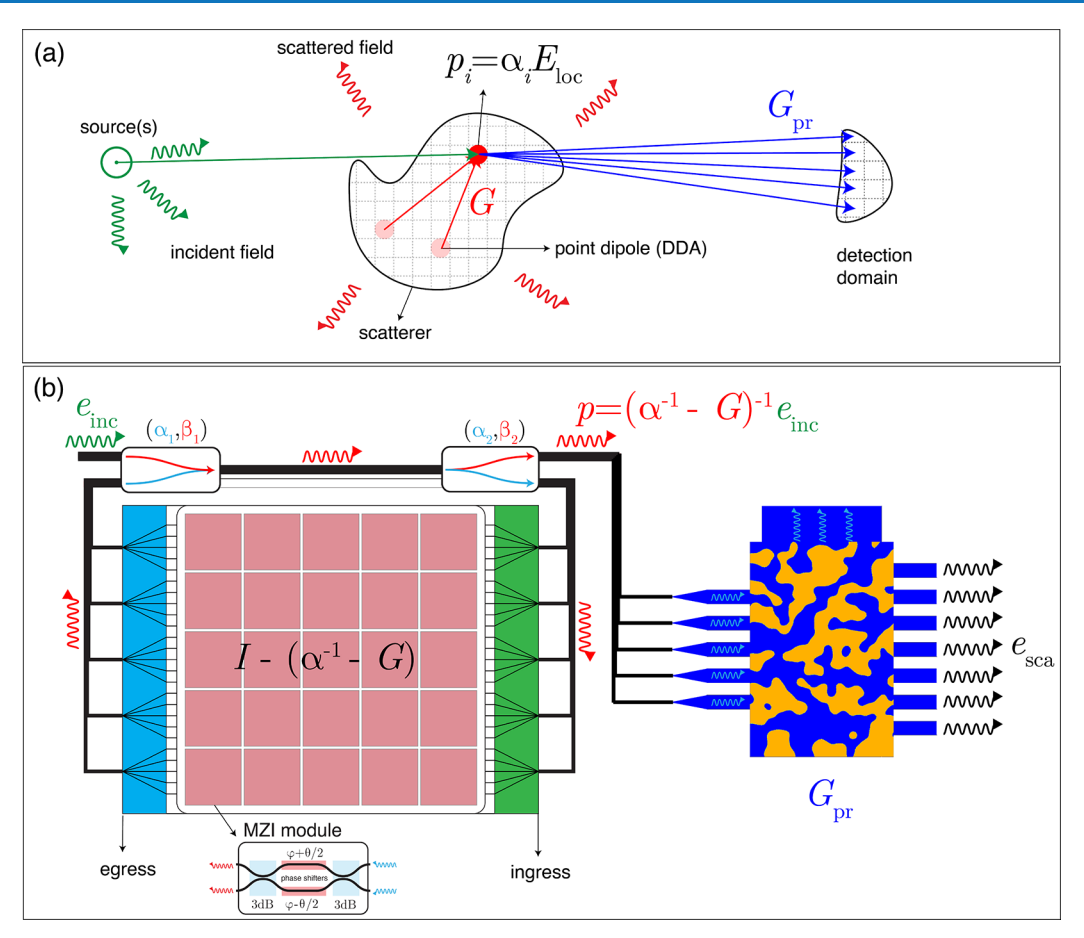


Figure 1. Proposed metadevice that emulates the forward scattering problem: (a) The physical problem that consists of the incident excitation (green arrows), the scattered field (red), and the scattered field obtained at a given set of detection points. Computing the scattered fields requires the matrix inversion for the determination of the induced dipole polarization vectors at the scatters due to the incident excitation, and a matrix-vector operation for the evaluation of the scattered field at the desired detection domain. (b) Our proposed device consists of the reconfigurable direct-complex-matrix (DCM) architecture involving reconfigurable multipliers (for matrix inversion) and the inverse-designed metastructure (for vector-matrix multiplication). The first emulates the interaction between the induced dipoles of the scatterers (following DDA), whereas the second evaluates the propagator.

product between the Green's propagator matrix and the induced polarization vector to compute the scattered fields. This part of our metadevice is formed using an inhomogeneous distribution of dielectric materials, whose optimized distribution is obtained using the method of inverse design. Finally, we validate the performance of the proposed design through simulations of a series of forward-scattering examples.

This Article is organized as follows: Formulated Overview gives a brief overview of the mathematical formalism for solving forward scattering problems using the method of discrete dipole approximation (DDA). In Metadevice Design, the details of the metadevice design are presented, that is, the tunable couplers and the inverse-designed stages. We then test, via simulation, the proposed device against two particular examples of a forward scattering problem in Examples and Discussion, that is, (a) an example of a scattering problem with various incident fields and permittivity profiles and (b) an example of a through-the-wall radar imaging problem. The summary and the concluding remarks are given in Summary and Conclusion.

#### FORMULATION OVERVIEW

We start with the standard integral representation of the electromagnetic scattering for a two-dimensional (2D) problem:

$$\mathbf{E}(\mathbf{r}) = \mathbf{E}_{inc}(\mathbf{r}) + \int_{S} \mathbf{G}(\mathbf{r}, \mathbf{r}') \chi(\mathbf{r}') \mathbf{E}(\mathbf{r}') d^{2}\mathbf{r}'$$
(1)

where  $E(\mathbf{r})$  and  $E_{\rm inc}(\mathbf{r})$  are, respectively, the total and the incident electric fields at the observation point  $\mathbf{r}$ ,  $G(\mathbf{r}, \mathbf{r}')$  is the 2D Green's function of the Helmholtz's equation, and  $\chi(\mathbf{r}')=\varepsilon_0(\varepsilon_r(\mathbf{r}')-1)$  is the susceptibility (sometimes referred to as contrast or scattering potential) of the object with relative permittivity  $\varepsilon_r(\mathbf{r}')$  and enclosed by the cross-sectional surface S as shown in Figure 1a. Here we have assumed that the surrounding medium is air with permittivity  $\varepsilon_0$ . Indeed, eq 1 is a Fredholm integral equation of the second kind that is often referred to as the Lippmann–Schwinger equation 12 and lies within the heart of many numerical electromagnetic methods, such as the discrete dipole approximation (DDA), 13,14 the contrast source inversion method (CSI), 15,16 the coupled dipole method, 17 and the Method of Moments (MoM).

We need to express eq 1 in terms of its equivalent discrete version using matrix/vector quantities. For this purpose we closely follow the DDA approach, a general method for solving

electromagnetic scattering problems of dielectric targets of arbitrary shapes and compositions. <sup>19</sup> The domain S that contains the 2D dielectric object is discretized in small scattering cells i = 1, 2, 3, ..., N, where each 2D cell exhibits an induced dipole moment  $\mathbf{p}_i$  that is generally proportional to the geometrical shape (here surface) and the associated permittivity at the ith cell (assuming piecewise homogeneous scatterers) and the local electric field (Figure 1a). The evaluation of the unknown induced dipole moments is the first goal of our approach. Each cell acquires its dipole moment due to the local electric field, that is,

$$\mathbf{p}_{i} = \alpha_{i} \mathbf{E}_{i}^{\text{loc}} \tag{2}$$

where the  $\mathbf{E}_i^{\mathrm{loc}}$  is the local electric field at the center of the cell i and  $\alpha_i$  is the polarizability that depends on the shape and the material composition of each 2D cell. In turn, the local field is generated by the incident field and the secondary fields generated from all the rest of the dipoles (other discrete cells) such that

$$\mathbf{E}_{i}^{\text{loc}} = \mathbf{E}_{i}^{\text{inc}} + \sum_{k \neq i}^{N} \mathbf{G}_{ik} \mathbf{p}_{k}$$
(3)

where  $\mathbf{E}_{i}^{\text{inc}}$  is the incident field at the target point i,  $\mathbf{p}_{k}$  is the polarization induced inside the target cell k and  $\mathbf{G}_{ik}$  is the 2D Green's function for calculating the fields, generated from  $\mathbf{p}_{k}$ , at the location of the target point i. In our case, we consider a two-dimensional (2D) problem with a transverse electric (TE) excitation. Therefore, the corresponding Green's function reads

$$\mathbf{G}_{ik} = \mathbf{G}(\mathbf{r}_i - \mathbf{r}_k) = -j \frac{k_0^2}{4\pi\epsilon_0} H_0^{(2)}(k_0 | \mathbf{r}_i - \mathbf{r}_k|)$$
(4)

where  $H_0^{(2)}(k_0|\mathbf{r}_i - \mathbf{r}_k|)$  is the Hankel function of the second type and 0th order and  $k_0 = \omega_0 \sqrt{\mu_0 \varepsilon_0}$  is the free-space wavenumber<sup>20</sup> (here we use the  $e^{j\omega t}$  convention). By combining eqs 2 and 3, we get the following expression:

$$\alpha_i^{-1} \mathbf{p}_i = \mathbf{E}_i^{\text{inc}} + \sum_{i \neq k}^N \mathbf{G}_{ik} \mathbf{p}_k$$
(5)

for which the unknown quantity is the dipole polarization induced inside the cells, that is,  $\mathbf{p}_{i}$  i=1,...,N. Using simple algebra, the above system can be arranged using the matrix formulation as follows:

$$p = (\text{diag}(\alpha^{-1}) - G)^{-1} e_{\text{inc}}$$
 (6)

where the lowercase quantities  $p = [\mathbf{p}_1, \mathbf{p}_2, ..., \mathbf{p}_N]^T$ ,  $\alpha = A_{\text{cell}} \epsilon_0 [\epsilon_1 - 1, \epsilon_2 - 1, ..., \epsilon_N - 1]$   $(A_{\text{cell}})$  is the cross-sectional area of a cell) and  $e_{\text{inc}} = [\mathbf{E}_1^{\text{inc}}, \mathbf{E}_2^{\text{inc}}, ..., \mathbf{E}_N^{\text{inc}}]^T$  are  $\mathbb{C}^{N \times 1}$  vectors,  $\text{diag}(\cdot)$  is the diagonal matrix operator, and G is a  $\mathbb{C}^{N \times N}$  Toeplitz matrix with zero diagonal entries (assuming a uniformly spaced discrete grid).

Finally, the scattered field observed at M specified discrete detection points (in general,  $M \neq N$ ) is given by

$$e_{\text{sca}} = G^{\text{pr}} p = G^{\text{pr}} (\text{diag}(\alpha^{-1}) - G)^{-1} e_{\text{inc}}$$
(7)

where  $G^{\text{pr}} \in \mathbb{C}^{M \times N}$  is the "propagator" Green's function matrix connecting the induced dipole polarization vectors of subscatterers (cells) and the detection points. Based on the

above matrix representations of the scattering problem we propose a specially designed wave-based reconfigurable metadevice that is able to simultaneously solve eq 6 and implement the vector-matrix operation of eq 7 for different excitations and for different scattering scenarios. It is worth emphasizing that, according to eq 6, the forward scattering problem requires a matrix inversion to evaluate the polarization density vectors induced in each scattering cell.

# ■ METADEVICE DESIGN

In this section we present the main results of our study. As sketched in Figure 1b, our proposed metadevice consists of two parts: (A) the matrix inversion part and (B) the vector-matrix multiplication part. For the first part we utilize a recently introduced Direct Complex Matrix (DCM) reconfigurable architecture properly connected to a feedback loop, capable of performing the desired matrix inversion in eq 6. For the second part we propose an inverse-designed metastructure that is able to conduct the vector-matrix product for emulating the propagator matrix,  $G^{pr}$  in eq 7.

Reconfigurable DCM Network Stage for Inverting Matrices. This stage, shown as the left panel of Figure 1b, follows the architecture introduced in ref 22. In particular, a given  $N \times N$  complex-valued matrix can be implemented in this device for inversion that has three sections: (a) the ingress, (b) the middle, and (c) the egress sections. The ingress section consists of N number of  $1 \rightarrow N$  signal splitters, each of which splits each of the N inputs into N outputs. All such  $N^2$  outputs of the ingress section are then properly routed to the middle section that consists of  $N^2$  dedicated tunable components, each of which consists of a combination of a phase shifter and an amplifier/attenuator, which we call a "multiplier". These  $N^2$ multipliers directly represent  $N^2$  elements of the matrix in eq 6 to be inverted. Finally, the  $N^2$  outputs of the middle sections are then routed to the egress section, that is, N number of  $N \rightarrow$ 1 combiners. As such the egress section is basically inverse of the egress section. Moreover, there is a feedback loop connecting the outputs to the inputs. (As an aside, it is worth pointing out that such combiners are not power combiners. Instead, the output of each  $N \to 1$  combiner is proportional to the fraction of the algebraic sum of complexvalued amplitudes of N input signals, and consequently, the output power is usually less than the sum of the input power. As a result, the remaining power goes to some "loss channel", for example, either dissipates in the element, scattered away from the system, reflected, or goes out of the system in unused channels. Consequently, we need to have amplifiers to bring the output signal level up to the desired value for the feedback system.)

For the feedback loop section, we used two identical couplers that split the input and output signal with a coupling ratio  $\beta_{1,2}$  and the through is  $|\alpha_{1,2}|^2 = 1 - |\beta_{1,2}|^2$ , (see Figure 1b and the Supporting Information). The output of the DCM stage estimates a value that is proportional to the induced dipole polarization vector p. In order to retrieve the actuall value of the polarization vector we need (a) to scale the input vector  $e_{\text{inc}}$  that is,  $e_{\text{inc}}/\beta_1$ , and (b) scale the output, that is,  $p_{\text{DCM}}/\beta_2$ . Therefore, from eq 6 the total scaling factor  $\frac{1}{\beta_1\beta_2}$  should be applied to the DCM output. Notice that in all examples presented below we assume couplers with -30 dB coupling  $(|\alpha_1|^2 = |\alpha_2|^2 = 0.999$  and  $|\beta_1|^2 = |\beta_2|^2 = 0.001$ ) requiring a scaling factor of  $\approx 10^3$  to be applied at the output of

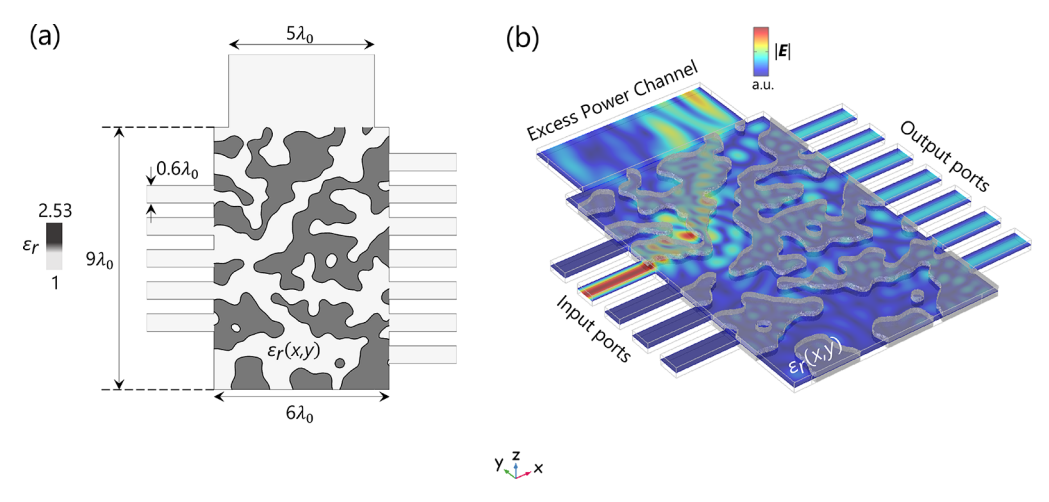


Figure 2. Inverse-designed metastructure: Inverse-designed structure designed for  $f_0 = 3$  GHz comprising five input and seven output ports for emulating the propagator matrix,  $G^{\rm pr}$ , of the configuration shown in Figure 3a. The size of the design region is  $(L_x, L_y) = (\delta \lambda_0, 9\lambda_0)$  and  $0.3\lambda_0$  along z direction. The material distribution is a function of (x, y) only. The input and output ports are single mode  ${\rm TE}^{10}$  waveguides. A multimode waveguide on top of the structure lets the excess power out. (a) The optimized distribution of polystyrene with  $\varepsilon_r = 2.53$  (dark gray regions) and air with  $\varepsilon_r = 1$  (light gray regions). (b) The magnitude of simulated electric field distribution inside the inverse-designed metastructure when the input port 2 is excited.

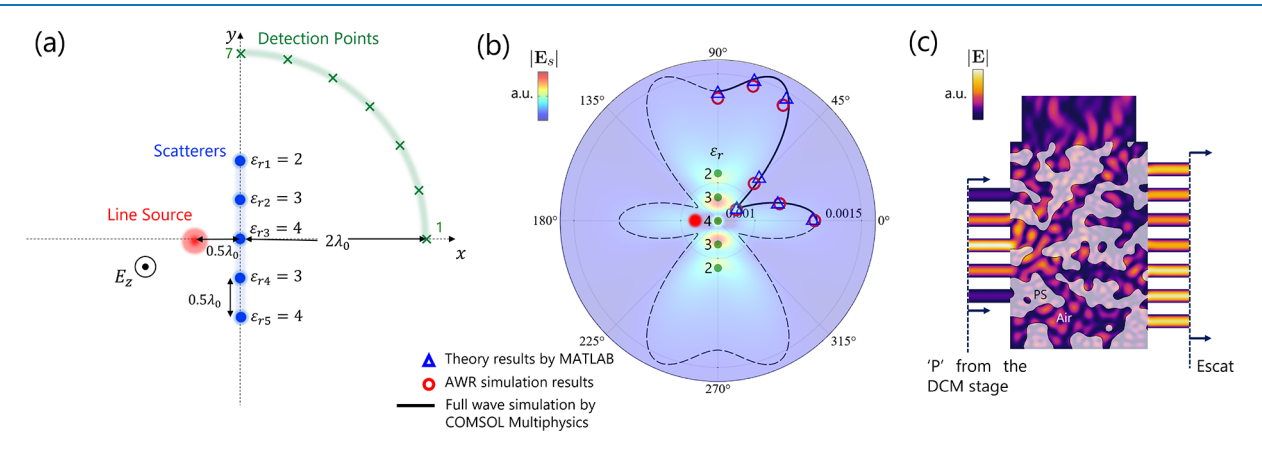


Figure 3. Example 1 and its simulation results: (a) Geometry of the forward scattering problem under investigation as the first example. Five two-dimensional 2D dielectric rods, with subwavelength cross sections, are illuminated by an infinitely long line electric current source with the out-of-plane electric field. The scattered fields are obtained at seven designated detection points on the circular path highlighted by green. (b) The scattered field distribution computed by full-wave simulation using the COMSOL Multiphysics v. 5.6. The scattered field data on the detection path obtained by the full-wave simulation (black solid curve), from the DDA calculation in Matlab (blue triangles), and from the simulated outputs of our proposed metadevice (with AWR Microwave Office, red circles) are compared on a polar plot. (c) Inverse-designed metastructure for emulating the propagator Green function. The inputs to this structure are excited with the complex amplitudes proportional to the p vector obtained by the DCM architecture. The mode amplitudes at the outputs are proportional to the scattered field complex amplitudes at the detection points.

this stage for the retrieval of the induced dipole polarization vector. (see the Supporting Information for evaluation of dimensionless quantities in our analysis.)

Overall, such a device can implement the desired matrix inversion, required in eq 6. <sup>22</sup> Since the N diagonal terms of this matrix depend on the relative permittivities of N scattering cells, these diagonal modules of the middle section can be reconfigured by changing the phase and magnitude of their transfer functions (using the phase shifters and the amplifiers/ attenuators in them) in order to accommodate different permittivities for these scatterers. (Note that we perform the inversion of the  $\operatorname{diag}(\alpha)^{-1} - G$  matrix, which requires that the eigenvalues of the kernel  $I - \operatorname{diag}(\alpha)^{-1} + G$  are inside the unit circle. Indeed, for the examples presented in this paper, this kernel has eigenvalues inside the unit circle. Therefore, for the set of permittivities we have in our examples, we need to tune

only N (diagonal entries) modules. However, in general, for different sets of scatterers and different relative positions (G matrix), one may need to perform preconditioning, as discussed in,<sup>22</sup> in order to guarantee that the eigenvalues are always within the unit circle. In such a case, we will need to reconfigure  $N^2$  modules for a new set of permittivities.)

In short, when the complex values of the incident fields at the location of *N* scatterers are inserted into the DCM stage of our metadevice, we evaluate the induced polarization vectors for different scattering scenarios represented by different material properties, for example, permittivities, of the individual scatterers and different incident excitations.

Inverse-Designed Metastructures for Emulating Propagator Matrix. In this section, we utilize the method of inverse design, 7,23-28 which is a density-based topology optimization technique using a gradient-descent approach

implemented by adjoint sensitivity analysis in COMSOL, to propose the wave-based inhomogeneous metastructures that emulate the propagator matrix  $G^{pr}$  (see also Supporting Information). Figure 2a presents an example of such a structure that represents the propagator matrix for a 2D scattering example with five scatterers and seven detection points (as shown in Figure 3a). This structure may consist of a metallic box with perfect electric conducting (PEC) walls, with five single-mode waveguides as the input ports and seven single-mode waveguides as its output ports. The inputs are excited with the complex amplitudes of the induced dipole polarization vectors (which are the outputs of the reconfigurable DCM network), and the complex-valued scattered fields at the detection points can be obtained (after applying the scale factor) at the outputs of this metastructure, according to  $e_{\text{sca}} = G^{\text{pr}} p$  (see Figure 2b).

The size of the design domain is  $6\lambda_0 \times 9\lambda_0 \times 0.3\lambda_0$  ( $\lambda_0$  is the free space wavelength corresponding to the design frequency  $f_0$ = 3 GHz). The size of the waveguides cross section is  $0.6\lambda_0 \times$  $0.3\lambda_0$  supporting TE<sup>10</sup> propagating mode only. The propagator matrix, Gpr, emulated with the inverse-designed metastructure, is the transmission block between the designated input and output ports in the scattering matrix. Since the metastructure is a lossless network, the scattering matrix must be unitary. However, the propagator matrix, that is, a portion of the scattering matrix, is generally not a unitary transmission block. Therefore, due to the nonunitary nature of  $G^{pr}$ , some of the input energy must couple to several "dump" modes other than the designated output ports. The number of dump modes for guiding the "excess energy" out of the metastructure must be large enough to satisfy the unitarity of the whole scattering matrix that contains the target transmission block as well. For that purpose, we placed a wide-enough waveguide (with a width of  $5\lambda_0$ ) that support multiple modes as "dump channels". In the design process, the objective is only defined over the transmission between the input and output ports, with no reflection back to the input ports. The dump channels act as extra degrees of freedom that ensure the unitary constraint and that the scattering matrix can be realized. The optimized material distribution inside the design region, for the example shown in Figure 3a, is shown in Figure 2a. The dark gray regions are assumed to be polystyrene with  $\varepsilon_{r,poly}$  = 2.53 and the light gray regions are air. The material distribution is only a function of (x, y) and it is invariant along the z direction. Figure 2b shows the norm of the simulated electric field distribution inside the optimized structure when the input port 2 is excited for the example shown in Figure 3a.

Since the elements of  $G^{\rm pr}$  only depend on the relative distances between locations of scattering cells and detection points, as long as the locations of the cells and the detection points are unchanged the designed metastructure can be used to compute the scattered fields for various forward scattering problems with different relative permittivity of the scatterers and various types of incident excitations.

In the next section, the simulation results for our proposed metadevice, which is the combination of the DCM stage and inverse-designed metastructure, are presented and evaluated for computing forward scattering in several examples. We show that the metadevice is capable of computing the complex amplitudes of the scattered fields at the detection points, for different incident radiations and various relative permittivities of the target scatterers. Due to the mathematical structure of the problem, there is a need for a matrix inversion (stage 1,

DCM) and a matrix-vector multiplication (stage 2, inverse-designed metastructure). In principle, the second stage can also be implemented with another DCM structure. However, while the DCM offers reconfigurability, its operation would require "active" components (amplifiers/attenuators, phase shifters, etc.), whereas an inverse-designed metastructure is a passive device. So instead of having two DCM structures, here in our work, we propose one DCM structure, which is reconfigurable, allowing different excitations and dielectric constants for the scatterers, and an inverse-designed passive structure that does not involve any active elements and thus is simpler in functionality.

# **EXAMPLES AND DISCUSSION**

As the first example, depicted in Figure 3a, we consider the 2D scattering from five infinitely long cylindrical dielectric rods (parallel with the z axis) that are separated by  $\lambda_0/2$ , placed along a linear grid on the y axis. The diameter of each rod is chosen to be deeply subwavelength,  $d = \lambda_0/50$ , to model each rod with a polarizability of  $\alpha_i = A_{\text{rod}} \varepsilon_0(\varepsilon_i - 1)$ , where  $A_{\text{rod}} =$  $\pi d^2/4$  is the cross-sectional area of the rod and  $\varepsilon_i$  is the relative permittvity of the rod i, i = 1, 2, ..., 5. In this example, the relative permittivities of the rods are chosen to be  $\varepsilon_r = \{2, 3, 4, 4, 6\}$ 3, 2, as shown in the figure. An infinitely long z-oriented electric line source, located  $\lambda_0/2$  away from the center of the array, is generating the incident electromagnetic field with an out-of-plane E-field polarization. The scattered fields generated from these five rods are to be evaluated at seven designated detection points positioned on a quarter section of a circle with radius of  $2\lambda_0$ , as shown in Figure 3a. As we discuss below our proposed metadevice can evaluate the scattered fields from this structure, evaluated at the detection points. The DCM stage of the metadevice is designed to allow the inversion of the matrix containing the information about the relative permittivities and locations of these five scatterers (see eq 6), and the inversedesigned metastructure section is designed to emulate the propagator part of eq 7 for this scattering problem. Figure 3c shows this inverse-designed metastructure. The DCM stage is simulated using the AWR Microwave Office and the wave interaction in the inverse-designed metastructure is simulated using the COMSOL Multiphysics v. 5.6 (see the Supporting Information). As depicted in Figure 1b, the complex-valued incident electric fields at the locations of five rods are considered as the inputs to the DCM stage, and the complexvalued induced dipole polarization amplitudes excited from the DCM stage are the inputs to the inverse-designed metastructures. Figure 3b depicts the magnitude of the scattered electric field, obtained from full-wave simulations using the COMSOL Multiphysics v. 5.6. The solid curve indicates this magnitude on the quarter circle of radius of  $2\lambda_0$ where the detection points are located. Moreover, we show (as blue triangle) the theoretical results for such scattered field amplitude as obtained from the analytical expression (eq 7) using Matlab, and the simulation results from the outputs of our proposed metadevice (shown as red circles). We note the good agreement among all three approaches (for the phase information and the comparison, see the Supporting Information). Figure 3c, shows the electric field distribution inside the inverse-designed metastructure and the relative mode amplitudes at the output ports (the results of which are shown by red circles in Figure 3b).

Since our metadevice is designed based on Green's function formulation in eq 7, the incident field could be arbitrarily

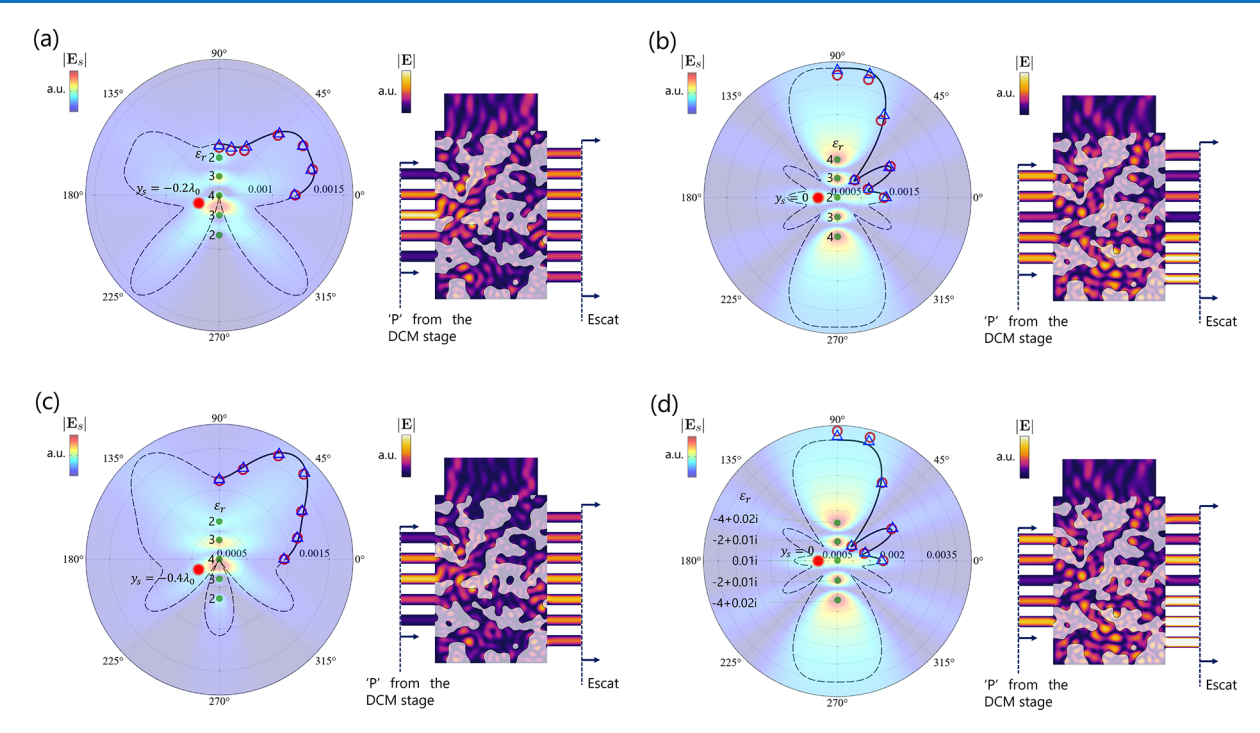


**Figure 4.** Examples 2 (first row) and 3 (second row): Different incident excitation and different sets of relative permittivities of the rods. Similar to the example of Figure 3, here we have the simulations results for the scattered fields (blue triangle Matlab results, red circle AWR Microwave Office simulation results, black line full wave simulations with COMSOL Multiphysics v. 5.6) for different incident radiations produced by a line source that is displaced by (a)  $0.2\lambda_0$  and (b)  $0.4\lambda_0$  downward relative to the center of the array. The second row shows the corresponding results for the modified relative permittivities for (c)  $\varepsilon_r = \{4, 3, 2, 3, 4\}$  and for (d)  $\varepsilon_r = \{-4 + j0.02, -2 + j0.01, j0.01, -2 + j0.01, -4 + j0.02\}$ .

chosen. Therefore, the same metadevice is capable of computing the scattered fields for all sorts of incident radiation, without a need to be redesigned. For demonstrating this capability, as the second set of examples here, we displace the line source and evaluate the new scattered fields. Figure 4a and b show the results for the line source displaced  $0.2\lambda_0$  and  $0.4\lambda_0$  downward relative to the center of the array, respectively. The panels next to the scattered field results show the electric field inside the inverse-designed metastructure and the mode amplitudes at the output ports. The good agreement among the scattered field data confirms the ability of our metadevice to evaluate scattering fields for this scattering problem for an arbitrary incident radiation. (For the phase information, see the Supporting Information.)

As mentioned earlier, our DCM stage is reconfigurable, and consequently it can be adjusted for different values of relative permittivities of the rods as long as the rods stay at their given locations. This latter condition, when added to the fact that the detection points are also fixed, guarantees that the inversedesigned metastructure can be reused without any need for redesigning. This allows our metadevice to compute the scattered fields at the detection points for arbitrary relative permittivities of rods and arbitrary incident radiation. This capability could be useful in optimization problems where one needs to evaluate the EM scattering for numerous different distributions of the relative permittivity of the object, for example, in the ground-penetrating radar (GPR) and subsurface scenarios involving inverse profiling of composite targets. 29,30 As the third set of examples, for the same 2, 3, 4} as a new set of dielectric constants for the rods. Next, we modify some of the reconfigurable diagonal elements in the middle stage of our DCM architecture to implement the new

matrix to be inverted in order to provide us with a new set of the polarization induced inside the objects according to their given relative permittivities. (Please see our comment about preconditioning in the section about the reconfigurable DCM stage.) Figure 4c shows the scattered field results for the new set of relative permittivities of the objects being illuminated by a line source  $\lambda_0/2$  away from the center of the array. Figure 4d shows the corresponding results for anther set of relative permittivities of  $\varepsilon_r = \{-4 + j0.02, -2 + j0.01, j0.01, -2 + j0.01, -2 +$ -4 + i0.02. Again, good agreement is noted among the scattered field magnitude results for both sets of relative permittivities, hence, verifying the capability of our metadevice to compute the scattered fields in forward-scattering problems with various relative permittivity profiles of the target scatterer. (For the phase information and the comparison, see the Supporting Information.)

As the fourth example, we demonstrate the capability of our metadevice for performing forward-scattering computations for through-the-wall imaging applications. The through-the-wall radar imaging (TWRI) is a technique for making images of targets behind visually opaque dielectric walls using microwaves. The scattered fields from targets propagate back to the receiver for postprocessing.  $^{31-35}$  One of the challenges of the TWRI is the computation time (particularly when many iterations in the forward scattering are needed in such computation), which is a determining factor in the applicability of an imaging method for real-time applications. 31,36 Here we show how an extension of our proposed metadevice can be utilized to do the forward-scattering computation for the TWRI. Since our device computes with waves (and thus may exhibit high wave speed), the required time for image reconstruction may be reduced considerably, especially if one is also interested in estimating the permittivity profiles of the

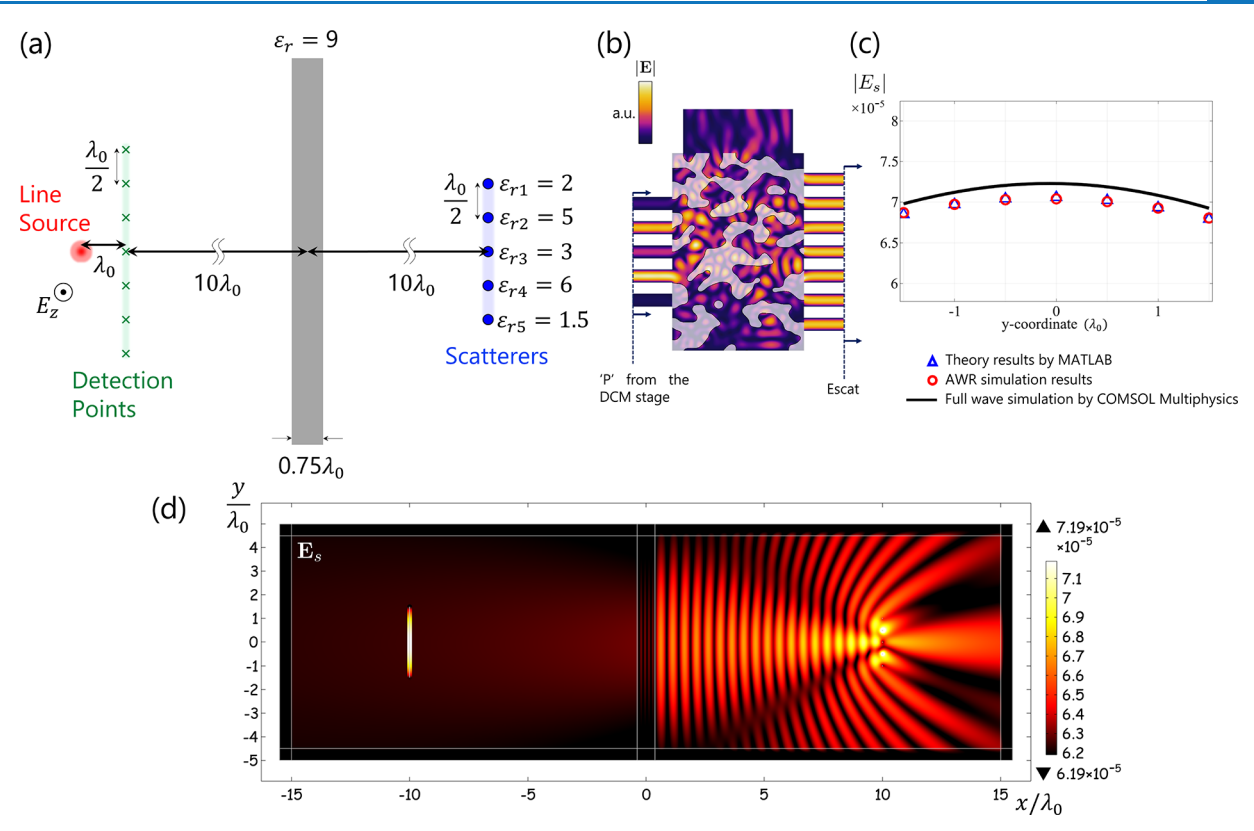


Figure 5. Through-the-wall-radar imaging (TWRI) application: (a) The geometry of a through-the-wall forward scattering problem. Five dielectric rods with spacing of  $\lambda_0/2$  and relative permittivities of  $\varepsilon_r = \{2, 5, 3, 6, 1.5\}$  from top to bottom, respectively, are hidden behind a dielectric wall with  $\varepsilon_r = 9$  and thickness  $d = 0.75\lambda_0$ . An infinitely line electric line source illuminates the scene and the scattered fields are detected at seven designated detection points with spacing of  $\lambda_0/2$ . The line source, detection points, and the scatterers are several wavelengths  $\sim 10\lambda_0$  away from the wall in order to use the far-field Green's function approximation in the presence of the wall. (b) The inverse-designed metastructure for emulating such Green's function,  $\mathbf{G}^{w}$ , for this problem (a). The input ports are excited with the complex amplitudes proportional to the induced diepole polarizations computed from the DCM stage. (c) The scattered field data at the detection points are evaluated with full-wave simulations in COMSOL Multiphysics v. 5.6 (black solid curve), in eq 9 in Matlab (blue triangles), and in the outputs of the metastructure simulated in AWR Microwave Office (red circles). (d) The normalized magnitude of the scattered electric field distribution simulated for the EM model shown in panel (a). The field values are normalized with respect to the incident wave, for which the amplitude of the line source that generates the incident cylindrical field is chosen such that  $\mathbf{E}_{\text{inc}} = (1 \text{ V/m})H_0^{(2)}(\mathbf{r} - \mathbf{r}_s)$ , where  $\mathbf{r}$  and  $\mathbf{r}_s$  are the observation and source position vectors. (Details on how Figure 5d is obtained can be found in the Supporting Information.)

targets behind or within the wall. As an aside, it is worth noting that in inverse profiling (e.g., GPR and subsurface applications), where one is concerned with finding both location and shape of an object as well as its material composition, the forward scattering problem becomes time-consuming, even when the target location is fixed.<sup>37</sup> In such scenarios, our proposed meta-device may become even more useful in reducing computation time.

A typical EM model of through-the-wall forward scattering for a single-layer dielectric wall is shown in Figure 5a. A 2D infinitely long line source with an out-of-plane electric field illuminates the scene and the detection points are positioned close to the source in a linear configuration, for receiving the scattered fields from the 2D target scatterers behind the wall. In order to use the far-field approximation of the wall's Green function the line source, scatterers, and the detection points are located several wavelengths away from the wall. The far-field Green function for a single-layer dielectric wall is as follows:

$$\mathbf{G}^{\mathrm{w}}(\mathbf{r} - \mathbf{r}_{s}) \approx T_{\mathrm{w}}\mathbf{G}^{\mathrm{pr}}(\mathbf{r} - \mathbf{r}_{s}) = -jT_{\mathrm{w}}\frac{k_{0}^{2}}{4\pi\epsilon_{0}}H_{0}^{(2)}(k_{0}|\mathbf{r} - \mathbf{r}_{s}|)$$
(8)

where  $G^w$  and  $G^{pr}$  are the 2D Green function in the presence of the wall and the 2D Green function in free-space, respectively.  $T_w$  is the wall's transmission coefficient for a normal incident plane wave and  $\mathbf{r}_s$  is the position of the line-source. The transmitted fields through the wall illuminate the objects behind it and the scattered fields propagate back through the wall to reach the detection points. Therefore, using the notation we used earlier, we may write the following formulation for calculating the scattered fields at the designated detection points:

$$e_{\text{sca}} = T_{\text{w}} G^{\text{pr}} p = T_{\text{w}} G^{\text{pr}} (\text{diag}(\alpha^{-1}) - G)^{-1} T_{\text{w}} e_{\text{inc}}$$
 (9)

Compared to eq 7 for a scattering problem in a free-space background, the only change we need to make for the present case with the wall is to include the transmission coefficient twice: one for the incident wave going through the wall to reach the scatterers and the other is for the scattered fields from the objects to reach the detection points. We note that the Green function in eqs 8 and 9 may be appropriately modified to redesign and tailor the metadevice for other forward scattering problems of interest such as those in intrawall imaging<sup>31</sup> on in GPR subsurface profiling.<sup>38</sup>

In Figure 5a, we consider a case of through-the-wall forward scattering. The thickness and relative permittivity of the wall are assumed to be  $0.75\lambda_0$  and  $\varepsilon_r = 9$ , respectively. Five 2D dielectric rods with diameter of  $d = \lambda_0/50$  are positioned as a linear array  $10\lambda_0$  away from the wall. The distance between adjacent cylinders is  $\lambda_0/2$  and the relative permittivities of the rods are  $\varepsilon_r = \{2, 5, 3, 6, 1.5\}$ . Seven detection points with spacing of  $\lambda_0/2$  are on the other side of the wall close to the source. The source is positioned  $\lambda_0$  away from the detection points. Figure 5d depicts the results of the full-wave simulation for the normalized scattered field distribution due to the scatterers using COMSOL Multiphysics v. 5.6 (see Supporting Information for details). Figure 5b presents the inversedesigned metastructure for emulating the far-field Green function with the wall present in the configuration shown in Figure 5a. Figure 5c shows the magnitude of scattered fields at the detection points using the COMSOL Multiphysics v. 5.6 full-wave simulation (black solid curve), the numerical results of eq 9 implemented in Matlab (blue triangles), and the simulation results for our metadevice (red circles). Close agreement is observed, verifying the capability of our proposed metadevice for performing forward-scattering computations for through-the-wall imaging. (For phase information and the comparison, see the Supporting Information.)

# SUMMARY AND CONCLUSION

In this work, we proposed a wave-based metadevice for computing electromagnetic forward scattering problems. The scattering object on which the integral equation is defined is discretized into small cells, and the induced dipole polarization inside the cells can be computed by inverting a matrix. We proposed a mesh of tunable couplers based on the DCM architecture for computing the matrix inversion and evaluating the polarization vector. The computed polarizations are fed into an inverse-designed metastructure that emulates the propagator Green's function for the computations of the desired scattered fields. The proposed metadevice is capable of computing the scattered fields for various scattering problems with different relative permittivity profiles of the object and different incident excitations. Although our proposed platform is customized for solving electromagnetic scattering problems, we can use the general concept behind this architecture to design other wave-based metastructure for solving other physical problems. One of the exciting potentials of this wave-based computing platform is the possibility of enhanced computation speed offered by the high speed of electromagnetic waves. Therefore, our architecture may significantly decrease the wait time for computations in applications where the numerical computation of a specific physical problem must be performed many times.

# ASSOCIATED CONTENT

# Supporting Information

The Supporting Information is available free of charge at https://pubs.acs.org/doi/10.1021/acsphotonics.2c00373.

The file includes: (1) Normalizing the DDA formulation, (2) Phase of the scattered field at the detection points, (3) Calculating the scattered fields from the hidden objects behind the wall in the TWRI problem, (4) Details of the inverse design, (5) Details of the system simulation (PDF)

#### AUTHOR INFORMATION

#### **Corresponding Author**

Nader Engheta — University of Pennsylvania, Department of Electrical and Systems Engineering, Philadelphia, Pennsylvania 19104, United States; orcid.org/0000-0003-3219-9520; Email: engheta@ee.upenn.edu

#### **Authors**

Vahid Nikkhah — University of Pennsylvania, Department of Electrical and Systems Engineering, Philadelphia, Pennsylvania 19104, United States

Dimitrios C. Tzarouchis – University of Pennsylvania, Department of Electrical and Systems Engineering, Philadelphia, Pennsylvania 19104, United States

Ahmad Hoorfar – Villanova University, Department of Electrical and Computer Engineering, Villanova, Pennsylvania 19085, United States

Complete contact information is available at: https://pubs.acs.org/10.1021/acsphotonics.2c00373

#### **Author Contributions**

§These authors contributed equally to this work.

#### Funding

This work is supported in part by the U.S. Air Force Office of Scientific Research (AFOSR) Multidisciplinary University Research Initiative (MURI) Grant Number FA9550-17-1-0002 and, in part, by the U.S. National Science Foundation (NSF) MRSEC Program under Award No. DMR-1720530.

#### **Notes**

The authors declare the following competing financial interest(s): N.E. is a strategic scientific advisor/consultant to Meta Materials, Inc.

#### REFERENCES

- (1) Miller, D. A. The role of optics in computing. *Nat. Photonics* **2010**, *4*, 406–406.
- (2) Miller, D. A. Attojoule optoelectronics for low-energy information processing and communications. *Journal of Lightwave Technology* **2017**, 35, 346–396.
- (3) Caulfield, H. J.; Dolev, S. Why future supercomputing requires optics. *Nat. Photonics* **2010**, *4*, 261–263.
- (4) Bogaerts, W.; Pérez, D.; Capmany, J.; Miller, D. A.; Poon, J.; Englund, D.; Morichetti, F.; Melloni, A. Programmable photonic circuits. *Nature* **2020**, 586, 207–216.
- (5) Zangeneh-Nejad, F.; Sounas, D. L.; Alù, A.; Fleury, R. Analogue computing with metamaterials. *Nature Reviews Materials* **2021**, *6*, 207–225.
- (6) Engheta, N.; Ziolkowski, R. W. Metamaterials: Physics and Engineering Explorations; John Wiley & Sons, 2006.
- (7) Piggott, A. Y.; Lu, J.; Lagoudakis, K. G.; Petykiewicz, J.; Babinec, T. M.; Vučković, J. Inverse design and demonstration of a compact and broadband on-chip wavelength demultiplexer. *Nat. Photonics* **2015**, *9*, 374–377.
- (8) Hughes, T. W.; Minkov, M.; Williamson, I. A.; Fan, S. Adjoint method and inverse design for nonlinear nanophotonic devices. *ACS Photonics* **2018**, *5*, 4781–4787.
- (9) Mohammadi Estakhri, N.; Edwards, B.; Engheta, N. Inverse-designed metastructures that solve equations. *Science* **2019**, 363, 1333–1338.
- (10) Camacho, M.; Edwards, B.; Engheta, N. A single inverse-designed photonic structure that performs parallel computing. *Nat. Commun.* **2021**, *12*, 1–7.
- (11) Zhu, H.; Zou, J.; Zhang, H.; Shi, Y.; Luo, S.; Wang, N.; Cai, H.; Wan, L.; Wang, B.; Jiang, X.; et al. Space-efficient optical computing

**ACS Photonics** Article pubs.acs.org/journal/apchd5

with an integrated chip diffractive neural network. Nat. Commun. 2022, 13, 1044.

- (12) Colton, D. L.; Kress, R.; Kress, R. Inverse Acoustic and Electromagnetic Scattering Theory; Springer, 1998; Vol. 93.
- (13) Purcell, E. M.; Pennypacker, C. R. Scattering and absorption of light by nonspherical dielectric grains. Astrophysical Journal 1973, 186,
- (14) Draine, B. T.; Flatau, P. J. Discrete-dipole approximation for scattering calculations. JOSA A 1994, 11, 1491-1499.
- (15) Wang, Y.; Chew, W. C. An iterative solution of the twodimensional electromagnetic inverse scattering problem. International Journal of Imaging Systems and Technology 1989, 1, 100-108.
- (16) Van Den Berg, P. M.; Kleinman, R. E. A contrast source inversion method. Inverse Problems 1997, 13, 1607-1620.
- (17) Lakhtakia, A. Macroscopic theory of the coupled dipole approximation method. Opt. Commun. 1990, 79, 1-5.
- (18) Kahnert, F. M. Numerical methods in electromagnetic scattering theory. Journal of Quantitative Spectroscopy and Radiative Transfer 2003, 79, 775-824.
- (19) Yurkin, M. A.; Hoekstra, A. G. The discrete dipole approximation: an overview and recent developments. Journal of Quantitative Spectroscopy and Radiative Transfer 2007, 106, 558-589.
- (20) Balanis, C. A. Advanced Engineering Electromagnetics; John Wiley & Sons, 2012.
- (21) Groth, S. P.; Polimeridis, A. G.; White, J. K. Accelerating the discrete dipole approximation via circulant preconditioning. Journal of Quantitative Spectroscopy and Radiative Transfer 2020, 240, 106689.
- (22) Tzarouchis, D.; Mencagli, M. J.; Edwards, B.; Engheta, N. Mathematical Operations and Equation Solving with Reconfigurable Metadevices. arXiv:2206.02549 [physics.app-ph] 2022, 1-19.
- (23) Molesky, S.; Lin, Z.; Piggott, A. Y.; Jin, W.; Vucković, J.; Rodriguez, A. W. Inverse design in nanophotonics. Nat. Photonics 2018, 12, 659-670.
- (24) Bendsoe, M. P.; Sigmund, O. Topology Optimization: Theory, Methods, and Applications; Springer Science & Business Media, 2003.
- (25) Piggott, A. Y.; Petykiewicz, J.; Su, L.; Vučković, J. Fabricationconstrained nanophotonic inverse design. Sci. Rep. 2017, 7, 1-7.
- (26) Sigmund, O. Topology optimization in nano-photonics. AIP Conference Proceedings 2009, 1176, 26-28.
- (27) Lu, J.; Boyd, S.; Vučković, J. Inverse design of a threedimensional nanophotonic resonator. Opt. Express 2011, 19, 10563-10570.
- (28) Lalau-Keraly, C. M.; Bhargava, S.; Miller, O. D.; Yablonovitch, E. Adjoint shape optimization applied to electromagnetic design. Opt. Express 2013, 21, 21693-21701.
- (29) Zhang, W.; Hoorfar, A. MIMO ground penetrating radar imaging through multilayered subsurface using total variation minimization. IEEE Transactions on Geoscience and Remote Sensing **2019**, *57*, 2107–2115.
- (30) Autieri, R.; D'Urso, M.; Isernia, T.; Pascazio, V. Inverse profiling via an effective linearized scattering model and MRF regularization. IEEE Geoscience and Remote Sensing Letters 2011, 8, 1021-1025.
- (31) Zhang, W.; Hoorfar, A.; Thajudeen, C. Two-and threedimensional fast intrawall imaging with microwave tomographic algorithm. International Journal of Antennas and Propagation 2018, 2018, 1-12.
- (32) Amin, M. G.; Ahmad, F. Compressive sensing for through-thewall radar imaging. Journal of Electronic Imaging 2013, 22, 030901.
- (33) Yemelyanov, K. M.; Engheta, N.; Hoorfar, A.; McVay, J. A. Adaptive polarization contrast techniques for through-wall microwave imaging applications. IEEE Transactions on Geoscience and Remote Sensing 2009, 47, 1362-1374.
- (34) Baranoski, E. J. Through-wall imaging: Historical perspective and future directions. Journal of the Franklin Institute 2008, 345, 556-
- (35) Zhang, W.; Hoorfar, A. Three-dimensional synthetic aperture radar imaging through multilayered walls. IEEE Transactions on Antennas and Propagation 2014, 62, 459-462.

- (36) Zhang, W.; Hoorfar, A. Three-Dimensional Real-Time Through-the-Wall Radar Imaging With Diffraction Tomographic Algorithm. IEEE Transactions on Geoscience and Remote Sensing 2013, 51, 4155-4163.
- (37) Imani, M. F.; Gollub, J. N.; Yurduseven, O.; Diebold, A. V.; Boyarsky, M.; Fromenteze, T.; Pulido-Mancera, L.; Sleasman, T.; Smith, D. R. Review of metasurface antennas for computational microwave imaging. IEEE Transactions on Antennas and Propagation 2020, 68, 1860-1875.
- (38) Hajebi, M.; Hoorfar, A. A multiscale optimization technique for large-scale subsurface profiling. IEEE Geoscience and Remote Sensing Letters 2021, 18, 1706-1710.

# **□** Recommended by ACS

# Optical Isolation by Temporal Modulation: Size, Frequency, and Power Constraints

Jacob B Khurgin.

MARCH 29, 2023

**ACS PHOTONICS** 

**Uniform Huygens Metasurfaces with Postfabrication Phase Pattern Recording Functionality** 

Elena Mikheeva, Julien Lumeau, et al.

MARCH 18, 2023

ACS PHOTONICS

READ **C** 

READ 2

Simultaneous Generation of Two Negatively Correlated Linearly Frequency-Modulated Pulses Based on an **Integrated Anti-Reflection Spectral Shaper** 

Dongyu Wang, Yiping Cui, et al.

MAY 02, 2023

**ACS PHOTONICS** 

READ **C** 

# Cylindrical Multimode Waveguides as Focusing **Interferometric Systems**

Wladislaw Michailow, David A. Ritchie, et al.

MAY 17, 2023

**ACS PHOTONICS** 

READ **C** 

Get More Suggestions >